Current Applied Physics 14 (2014) 1401–1410

Contents lists available at ScienceDirect

Current Applied Physics

journal homepage: www.elsevier.com/locate/cap

Computational investigation of low band gap dyes based on 2-styryl-5-phenylazo-pyrrole for dye-sensitized solar cells

Samaneh Bagheri Novir, Seyed Majid Hashemianzadeh*

Molecular Simulation Research Laboratory, Department of Chemistry, Iran University of Science & Technology, Tehran, Iran

ARTICLE INFO

Article history:
Received 9 May 2014
Accepted 27 July 2014
Available online 8 August 2014

Keywords:
Dye-sensitized solar cell
Time-dependent density functional theory
Electronic structure
Lifetime
TiO_2

ABSTRACT

In this work, the geometry, electronic properties and absorption spectra of low band gap organic dyes based on 2-styryl-5-phenylazo-pyrrole, C1, C2 and S dyes were theoretically investigated via DFT and TD-DFT in the gas phase and in solution. Theoretical calculations have been also carried out on the adsorption of these dyes on the TiO_2 anatase (101) surface that show bidentate bridging is preferred adsorption mode in these dyes. Highest charge populated in the acceptor group, longest lifetime of the first excited state, highest electronic coupling constant ($|V_{RP}|$) of the S dye and the most negative shift of the conduction band of TiO_2 due to the adsorption of the S dye on TiO_2 (ΔE_{CB}) show that these parameters are favorable to increase V_{oc}. The calculated results of these dyes demonstrate that theoretical calculations are useful not only in the description of these properties, but also in the design of new sensitizers.

1. Introduction

Solar energy is the most plenteous source of energy on earth, and its conversion into electricity, through photoelectrochemical solar cells, is generally regarded as the most appropriate method to solve the global energy crisis, owing to its massive reserves and pollution-free character. Although commercially available solar cells are currently based on inorganic silicon semiconductors, but their large-scale application has been limited due to the high cost of high-purity silicon. Among all the renewable energy technologies, the nanocrystalline dye-sensitized solar cells (DSSCs) which were presented by O'Regan and Grätzel in 1991, have attracted a lot of attention due to their potentially low fabrication costs, environmentally friendly components, relatively high conversion efficiencies and flexibility in their manufacture and employment [1–6]. In DSSCs process, light is absorbed by the dye anchored on the TiO_2 surface and then electrons from the excited dye inject into the conduction band of the TiO_2, generating an electric current. The oxidized dye is then reduced by electron transfer from the electrolyte, commonly based on the redox couple I^-/I_3^- in an organic solvent [6–9]. Up to now, two kinds of dyes have been studied extensively as sensitizers, metal–organic complexes and metal-free organic dyes. Metal–organic complexes, mainly the noble metal ruthenium polypyridyl complexes, have provided the highest performances, with solar energy to electrical energy conversion efficiencies beyond 11% [6,8,10]. Recently, more attention has been directed to the use of metal-free organic dyes in DSSCs because of no noble metal resource limitation, their high molar absorption coefficient, relatively simple synthetic procedure, various structures, the tunable absorption spectral response from the visible to the near infrared (NIR) region, environmentally friendly and economical production techniques [7,11,12]. Organic dyes in DSSCs generally consist of an electron donor, an electron acceptor, a π-conjugated bridge between the donor and acceptor, and/or an anchoring group. Light absorption causes an intramolecular charge transfer from the donor group to the acceptor group, through the π-bridge [13,14]. Metal-free organic dyes used in DSSCs must have suitable levels for the HOMO and the LUMO of the sensitizer matching the iodine redox potential and the conduction band edge level of the TiO_2. The energy level of the LUMO of the dye must be higher (more negative) than the conduction band of the TiO_2 (−4.1 eV). On the other hand, the energy level of the HOMO of the dye must be lower (more positive) than the I^-/I_3^- redox potential (−4.80 eV) [11,15,16].

The structure and physical properties of sensitizers are very important to improve the efficiencies of organic dye-based DSSCs. The conjugation across the donor and anchoring groups, and good electronic coupling between the LUMO of the dye and the conduction band of TiO_2 is useful for high electron-transfer rates.

* Corresponding author. Tel.: +98 21 77240287; fax: +98 21 77491204.
E-mail addresses: hashemianzadeh@yahoo.com, hashemianzadeh@iust.ac.ir (S.M. Hashemianzadeh).

http://dx.doi.org/10.1016/j.cap.2014.07.016
1567-1739/

Consequently, decreasing the energy of the charge-transfer transition is necessary. Pyrrole group, as an electron-rich heteroaromatic ring, has been used as a conjugated bridge in organic dyes. On the other hand, azo dyes are a well-known class of compounds containing an N=N double bond and due to their ability to absorb visible light, they have been extensively used in organic photoactive materials due to their excellent optical switching properties, high solution process abilities and good chemical stabilities. Over the past decade, azo dyes based polymers and materials have drawn a considerable amount of attention. Among the known azo dyes, azopyrroles are important. They have obvious bathochromic absorptions compared to azobenzene dyes [11,17,18]. Recently, three new dyes C1, C2 and S based on 2-styryl-5-phenylazo-pyrrole (Fig. 1), have been synthesized by Mikroyannidis et al., that C1 and C2 dyes contain one and two carboxy anchoring groups, respectively, and S dye has one sulfonic acid anchoring group. In these dyes, substituted-phenylazo at one side and cyanovinylene 4-nitrophenyl at the other side of the pyrrole ring, extended the absorption band of the dyes into the near infrared region, which is a favorable feature for DSSCs. The hexyl chain in these dyes enhanced the solubility of the dyes [11]. Theoretical calculations are useful in the description of the physical properties and disclose the relationship among the performance, structures and the properties of dye sensitizers. They could also help in the design of new sensitizers with the better performance [19,20]. In this work, the geometries, electronic properties, electronic transition, oxidation potential, the free energy changes of electron injection and electronic absorption spectra of C1, C2 and S, were studied by using density functional theory (DFT) and time-dependent DFT (TD-DFT) methods. In order to calculate and compare the adsorption energies of different adsorption mode of the dyes and also studying TiO_2 conduction band energy shift upon the dyes adsorption, theoretical calculations have been carried out on the adsorbed dyes onto the TiO_2 anatase (101) surface. Because of the limitation of current computational capacity, the smallest possible TiO_2 anatase (101), the $(TiO_2)_{24}$, has been used in this work. The surface area of the $(TiO_2)_{24}$ is suitable for the anchoring groups of the dyes to anchor onto.

Finally, the computational results were compared and correlated with the available experimental information and allow us to describe qualitatively some effective factors in the efficiency of these dyes and theoretically explain why the S dye has the larger efficiency than C2 and C1 dyes.

2. Computational methods

All calculations on the free dyes in this work were performed by the Gaussian 03 program package [21]. The ground state geometries of C1, C2 and S were optimized at the DFT level of theory with Becke's [22] three parameters hybrid functional and Lee–Yang–Parr [23] correlation functional (B3LYP) [22] by using 6-311+G(d,p) basis set. Vibrational Frequency calculations were carried out on the optimized geometries at the same level to show that all optimized geometries reached a stationary point. Natural bond orbital (NBO) calculations also have been performed at the same level on optimized structures. Time-dependent DFT (TD-DFT) calculations for the lowest 30 singlet–singlet transitions at the optimized geometry in the ground state were performed with the hybrid functional B3LYP and 6-311+G(d,p) basis sets for calculation of excitation energies and oscillator strengths of these dyes. The free energy change (in eV) for electron injection from excited dyes to TiO_2 surface, can be calculated from Rehm Weller equation [16,24]:

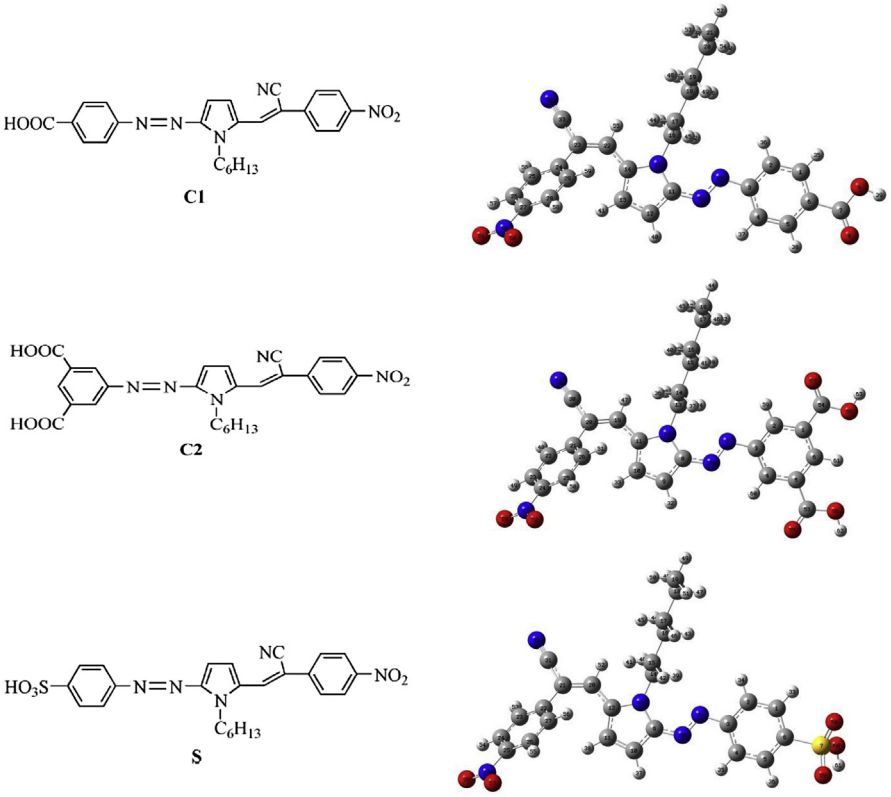

Fig. 1. Schematic and optimized geometrical structures of dyes C1, C2 and S with B3LYP/6-311+G(d,p).

Table 1
Selected bond lengths (in Å), bond angles (in °) and dihedral (in °) of the C1, C2 and S dyes.

C1		C2		S	
C3–N10	1.41261	C3–N7	1.41551	C3–N8	1.41345
N10–N32	1.26742	N7–N29	1.26592	N8–N30	1.26764
C11–N32	1.36851	C8–N29	1.36861	C9–N30	1.36678
C11–C12	1.40354	C8–C9	1.40318	C9–C10	1.40395
C12–C13	1.38641	C9–C10	1.38659	C10–C11	1.38591
C13–C14	1.40619	C10–C11	1.40623	C11–C12	1.40669
C14–C22	1.43697	C11–C19	1.43739	C12–C20	1.43799
N10–N32–C11	119.2	N7–N29–C8	119.2	N8–N30–C9	119.3
C3–N10–N32	114.5	C3–N7–N29	114.3	C3–N8–N30	114.3
N32–C11–C12	121.1	N29–C8–C9	121.2	N30–C9–C10	121.1
C13–C14–C22	129.9	C10–C11–C19	129.9	C11–C12–C20	129.9
C14–C22–C23	129.4	C11–C19–C20	129.3	C12–C20–C21	129.3
N10–N31–C11–C12	−176.3	N7–N29–C8–C9	−174.6	N8–N30–C9–C10	−176.8
C3–N10–N32–C11	−179.8	C3–N7–N29–C8	−179.3	C3–N8–N30–C9	179.9
C13–C14–C22–C23	21.8	C10–C11–C19–C20	22.1	C11–C12–C20–C21	21.6

$$\Delta G^{\text{inject}} = E_{\text{OX}}^{\text{dye}*} - E_{\text{CB}}^{\text{TiO}_2}, \tag{1}$$

where $E_{\text{OX}}^{\text{dye}*}$ is the oxidation potential energy of the dyes in the excited state and $E_{\text{CB}}^{\text{TiO}_2}$ is the reduction potential of the conduction band of the TiO_2 [24,25]. The $E_{\text{CB}}^{\text{TiO}_2} = -4.1$ eV adopted in this work obtained from experiment [11]. $E_{\text{OX}}^{\text{dye}*}$ can be expressed by:

$$E_{\text{OX}}^{\text{dye}*} = E_{\text{OX}}^{\text{dye}} - E_{00} + \omega_r. \tag{2}$$

In this definition, $E_{\text{OX}}^{\text{dye}}$ is the oxidation potential energy of the dyes in the ground state, E_{00} is vertical excitation energy and ω_r is a coulombic term that can be negligible [16,25,26], so $E_{\text{OX}}^{\text{dye}*}$ is approximately expressed as: $E_{\text{OX}}^{\text{dye}} - E_{00}$. The free energy change of the dyes is calculated for evaluating spontaneous electron injection from dye to TiO_2. Solvent effects affect on geometrical parameters and electronic structures and the related properties of the dyes [27,28]. The solvation effects were evaluated using the conductor polarizable continuum model (CPCM) [29] in the Gaussian 03 program, for both geometry optimizations and TD-DFT calculations.

The lifetime of the first excited state (τ) is a main factor for considering the efficiency of charge transfer of organic dyes. In this study, the lifetime of an excited state was estimated by:

$$\tau = \frac{1}{A_{k,k'}}, \quad A_{k,k'} = \frac{4e^2 \Delta E_{k',k}^3}{3\hbar^4 C^3} |r_{k,k'}|^2, \tag{3}$$

where $A_{k,k'}$ is Einstein coefficient for spontaneous emission, $\hbar$ is the reduced Planck's constant, c is the speed of light in vacuum, e is the elementary charge, $\Delta E_{k,k'}$ and $r_{k,k'}$ are the transition energy and transition dipole moment from states k to k', respectively [30,31]. The next step in this work was to study the dye–TiO_2 configurations. To do so, we produced a $(TiO_2)_{24}$ with the anatase (101) surface. The anatase TiO_2 (101) surface used in the present work, consists of a periodically repeated slab of $3 \times 1 \times 2$ slabs containing altogether 24 Ti and 48 O atoms, and a vacuum space of 30 Å above the slab. All structures of dye–TiO_2 were optimized at the level of DFT/BLYP with a plane wave basis set (cutoff energy = 40 Ry) and Vanderbilt ultra-soft pseudopotentials [32–35] with the CPMD code [36].

3. Results and discussion

3.1. Ground-state optimized geometries

The sensitizers C1, C2 and S based on 2-styryl-5-phenylazo-pyrrole contain one and two carboxy anchoring groups and sulfonic acid anchoring group, respectively. In these dyes 1-hexylpyrrole is the central unit which is connected with cyanovinylene 4-nitrophenyl at one side and with substituted-phenylazo at the other side of the pyrrole ring [11]. The schematic and optimized ground-state geometries of C1, C2 and S are shown in Fig. 1, and the selected bond lengths, bond angles and dihedral angles are listed in Table 1. All the CC lengths in the pyrrole and phenyl rings, the NN length in azo group and the CN length in substituted-phenylazo which is connected to pyrrole ring are between the distance of a single bonded and a double bonded, indicating that there exists extensive delocalization throughout the molecule. The substituted-phenylazo in C1, C2 and S is located to be almost coplanar with the pyrrole ring, as represented by the N10–N32–C11–C12, N7–N29–C8–C9 and N8–N30–C9–C10 dihedral angles, respectively, while the coplanarity between the cyanovinylene 4-nitrophenyl group and pyrrole ring is destroyed, as shown by the C13–C14–C22–C23, C10–C11–C19–C20 and C11–C12–C20–C21 angles, respectively. Thus, the pyrrole ring and substituted-phenylazo are fully conjugated and the electron transfer from the 1-hexylpyrrole to substituted-phenylazo is more favorable.

3.2. Electronic structures

C1, C2 and S were soluble in common organic solvents such as THF, dichloromethane and chloroform due to the hexyl chain [11]. The ground state structures of these dyes were optimized at the B3LYP/6-311+G(d,p) level in vacuum and the solvents. The E_{HOMO},

Table 2
The highest occupied molecular orbital energies (E_{HOMO} (in eV)), the lowest unoccupied molecular orbital energies (E_{LUMO}(in eV)) and HLG (in eV) of all dyes obtained at the B3LYP/6-311+G(d,p) level.

Dye	E_{HOMO}	E_{LUMO}	HLG
C1			
Vacuum	−6.36	−3.61	2.75
THF	−6.16	−3.44	2.72
Dichloromethane	−6.16	−3.44	2.72
Chloroform	−6.19	−3.46	2.73
C2			
Vacuum	−6.39	−3.57	2.82
THF	−6.19	−3.43	2.76
Dichloromethane	−6.18	−3.43	2.75
Chloroform	−6.21	−3.44	2.77
S			
Vacuum	−6.54	−3.74	2.80
THF	−6.25	−3.50	2.75
Dichloromethane	−6.24	−3.50	2.74
Chloroform	−6.29	−3.53	2.76

E_{LUMO} and HLG ($E_{LUMO} - E_{HOMO}$) of all these dyes in vacuum and the various solvents are listed in Table 2. The E_{HOMO} and the E_{LUMO} for all dyes in various media are in increasing order: vacuum < chloroform < THF < dichloromethane, and the HLG for these dyes in these phases is in the opposite order. It can be noted that the various environments play a main role in stabilization of E_{HOMO} and E_{LUMO} and the most positive value of HLG is found in vacuum. For the C1, C2 and S dyes, THF and dichloromethane effects induced that the HOMO increased about 0.20 eV, 0.21 eV and 0.29 eV, and LUMO increased about 0.17 eV, 0.14 eV and 0.24 eV, respectively. Chloroform effects induced that the HOMO levels of C1, C2 and S increased about 0.17 eV, 0.18 eV and 0.25 eV, and LUMO increased about 0.15 eV, 0.13 eV and 0.21 eV, respectively. These results indicate that the effects of THF and dichloromethane on E_{HOMO} and E_{LUMO} are almost equal while chloroform effects are lower than THF and dichloromethane. Since the results of the experimental work are reported in THF solvent, we adopted THF in this computational study.

The calculated HOMO energy levels of C1, C2 and S in the gas phase are located at −6.36, −6.39 and −6.54 eV, and their corresponding LUMO energy are located at −3.61, −3.56 and −3.74 eV, respectively. There are same electron donors in the three dyes, so the difference of the HOMOs is small. The difference of the LUMOs is due to their different electron anchoring groups, one carboxy anchoring group for C1, two carboxy anchoring groups for C2 and one sulfonic acid anchoring group for S. The calculated LUMOs of C1, C2 and S, are almost close to experimental values and the order of the calculated LUMOs of C1, C2 and S in THF (S(−3.50 eV) < C1(−3.44 eV) < C2(−3.43 eV)) is consistent with the order of experimental values (S(−3.28 eV) < C1(−3.26 eV) < C2(−3.25 eV)) [11].

Usually the energy gap between the LUMO of the dye and the conduction band of the TiO_2, must be more than 0.2 eV for effective electron injection [5,37]. Calculated results show that LUMO energy levels of the three dyes are higher than that of TiO_2 conduction band edge (−4.1 eV) and the energy gap between them is more than 0.2 eV, thus molecules in the excited states of C1, C2 and S have a strong ability to inject electrons into TiO_2 electrodes. The HOMOs of all three dyes are lower than reduction potential energy of the I^-/I_3^- electrolyte (−4.8 eV), therefore these dyes that lose electrons could be restored by getting electrons from the electrolyte. Since the energy gap between the LUMO level and the conduction band of the TiO_2 is different for all these dyes, consequently the electron injection efficiency is different of all DSSCs [11].

Natural bond orbital (NBO) calculation was performed in order to analyze the charge populations and characterize the intramolecular charge transfer of C1, C2 and S. The natural charges of each group are the sum of every atomic natural charge in the group [38]. Table 3 shows the natural charges of 1-hexylpyrrole, cyanovinylene 4-nitrophenyl and substituted-phenylazo in C1, C2 and S. These data indicate that the cyanovinylene 4-nitrophenyl and substituted-phenylazo are acceptors while the 1-hexylpyrrole is a donor. In all these dyes, the natural charges that populated in substituted-phenylazo acceptor groups are higher than the natural charges of cyanovinylene 4-nitrophenyl, indicating that the electron-drawing strength of substituted-phenylazo groups are higher than cyanovinylene 4-nitrophenyl group. Since substituted-phenylazo in all the dyes, is almost coplanar with the pyrrole bridge, while the coplanarity between the cyanovinylene 4-nitrophenyl group and pyrrole bridge is destroyed. It is found that substituted-phenylazo acceptor groups are anchoring groups in these dyes. Thus, there are the main charges transferred from the electron donor (1-hexylpyrrole) to the electron acceptor (substituted-phenylazo) for these dyes.

Table 3
Natural charges (e) of different groups in the dyes C1, C2 and S.

Dyes	1-Hexylpyrrole	Cyanovinylene 4-nitrophenyl	Substituted-phenylazo
C1	0.37006	−0.08992	−0.30152
C2	0.37343	−0.08695	−0.30789
S	0.08195	−0.29174	−0.33617

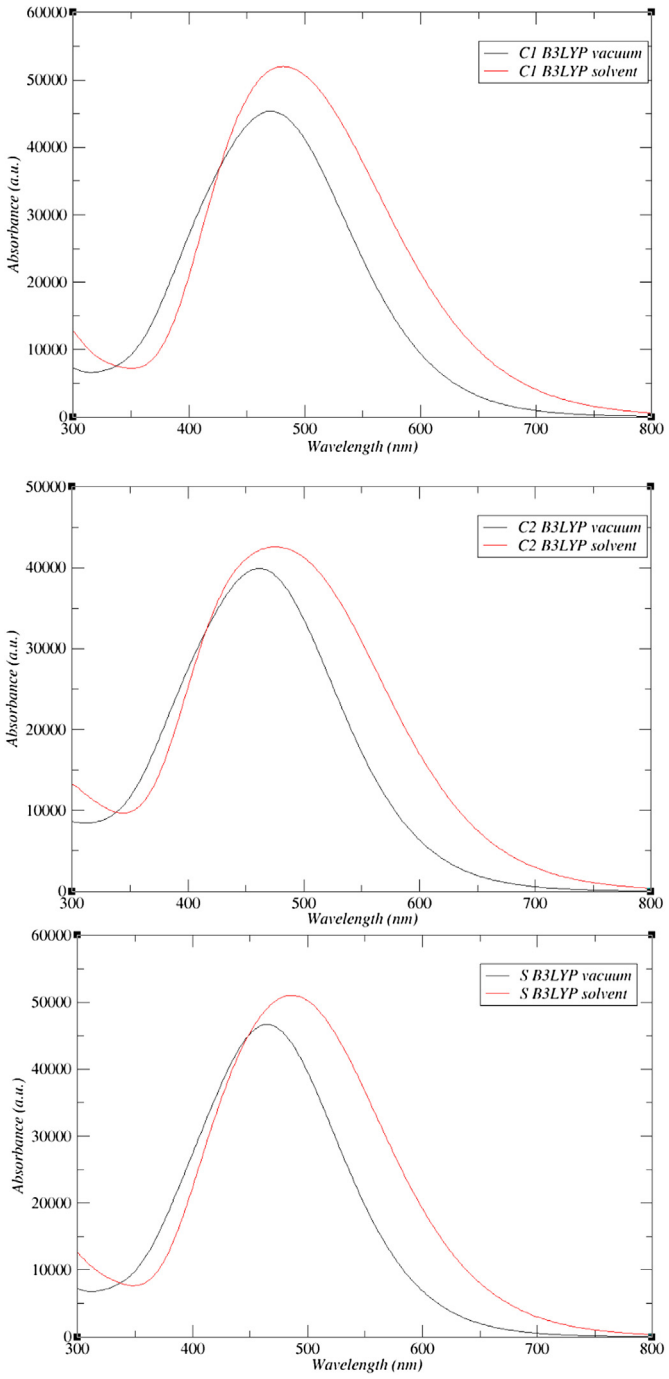

Fig. 2. Simulated absorption spectra of C1, C2 and S in the gas phase and THF solution at the B3LYP/6-311+G(d,p).

3.3. Electronic absorption spectra

Electronic absorption spectra of the C1, C2 and S dyes were performed using TD-DFT calculations. TD-DFT excited state calculations with the hybrid functional B3LYP and 6-311+G(d,p) basis set, based on the optimized geometries of B3LYP/6-311+G(d,p), were carried out on the 30 lowest spin-allowed singlet–singlet transitions for the dyes in vacuum and the solvents. The simulated UV–vis absorption spectra of the C1, C2 and S dyes calculated using B3LYP/6-311+G(d,p) in the gas phase and THF solvent, are shown in Fig. 2. UV–vis spectra were illustrated using the software Grace-5.1.23 [39]. The maximum wavelengths (λ_{max}) of C1, C2 and S in the gas phase and THF that calculated by TD-DFT are shown in Table 4. The TD-DFT results of the dyes have lower λ_{max} than the experimental results [11]. The discrepancy between experiment and TD-DFT calculations may be resulted from DFT exchange and correlation functional and the computational model of solvent effects [7,10]. Since of experimental measurements of electronic absorption spectra are usually performed in solution and solvent could affect the geometry and electronic structure as well as the properties of molecules, it is difficult to make that the TD-DFT calculation is consistent with quantitatively. Though the discrepancy is existed, the TD-DFT calculations are capable of describing the spectral features of these dyes because of the qualitative agreement with experiment [38]. The results show that the calculated λ_{max} with TD-DFT in solvent is much closer with experimental data than that in vacuum. Inclusion of solvent shifts the absorption bands of these dyes toward longer wavelength range. The HOMO–LUMO gap of these dyes in THF at B3LYP/6-311+G(d,p) level (Table 2) is smaller than that in vacuum. So it induces the red-shift of the absorption as compared with that in vacuum. Solvent effects increase the oscillator strength of the dyes as well [40].

To get the microscopic information about the electronic transitions, and since the absorption band in visible and near-UV region is the most important region for photo-to-current conversion, the wavelengths, oscillator strengths, transition energies of singlet–singlet transitions of the absorption bands with the wavelength longer than 400 nm, and the oscillator strength larger than 0.01 in THF solvent are listed in Table 5. As shown, there is an absorption band for C1 in 530.85 nm with oscillator strength of 0.625 which is a mixture of H → L (67%), H − 1 → L (23%) and H − 1 → L + 1 (8%) transitions; there is an absorption band for C2 in 520.67 nm with oscillator strength of 0.717 which is a mixture of H → L (86%), H − 1 → L (7%) and H − 1 → L + 1 (4%) transitions, and there is an absorption band for S in 516.92 nm with the oscillator strength of 0.475 which is a mixture of H → L (48%), H − 1 → L (38%) and H − 1 → L + 1 (10%) transitions. For the dyes the HOMO and HOMO − 1 are π orbitals whereas LUMO and LOMO + 1 are π* orbitals. Therefore, these absorption bands are assigned to the π → π* transitions.

The simulated absorption spectra by B3LYP/6-311+G(d,p) in THF for the C1, C2 and S dyes are shown in Fig. 3. The calculated results with TDDFT are in qualitative agreement with those of the experiment, and the λ_{max} shifted toward lower wavelengths (blue-shift) when going from C1 to C2 and S with respect to the experiment, although the discrepancy in absorption wavelengths exists.

Table 4
Maximums of absorption spectra (λ_{max}) of C1, C2 and S in the gas phase and THF solution calculated by TD-DFT at the B3LYP/6-311G+(d,p) level.

Dyes	λ_{max} (gas)	λ_{max} (THF)	λ_{max} (exp)
C1	514.45	530.85	625
C2	499.84	520.67	615
S	475.73	516.92	602

Table 5
Excitation energies, oscillator strengths, lifetimes for the first excited states (τ), light harvesting efficiency (LHE), $|V_{RP}|$, EBE and electronic transition configurations of the C1, C2 and S dyes calculated by TD-DFT at the B3LYP/6-311+G(d,p) level in THF.

Dyes	Excitation energy (eV/nm)	f	Lifetime (τ)/ns	LHE	$\lvert V_{RP}\rvert$	EBE	Configuration
C1	2.34/530.85	0.625	6.75	0.76	1.08	0.38	H → L (67%)
							H − 1 → L (23%)
							H − 1 → L + 1 (8%)
	2.45/505.22	0.2521					H − 1 → L (48%)
							H − 1 → L + 1 (13%)
							H → L (27%)
							H → L + 1 (10%)
	2.78/444.74	0.8185					H − 1 → L (4%)
							H → L (6%)
							H → L + 1 (88%)
C2	2.38/520.67	0.7171	5.66	0.81	1.09	0.37	H → L (86%)
							H − 1 → L (7%)
							H − 1 → L + 1 (4%)
	2.51/493.39	0.0741					H − 1 → L (59%)
							H − 1 → L + 1 (23%)
							H → L (9%)
							H → L + 1 (5%)
	2.87/431.17	0.7191					H − 1 → L (3%)
							H → L (3%)
							H → L + 1 (92%)
S	2.39/516.92	0.4757	8.41	0.67	1.13	0.35	H → L (48%)
							H − 1 → L (38%)
							H − 1 → L + 1 (10%)
	2.43/510.02	0.0741					H − 1 → L (39%)
							H − 1 → L + 1 (10%)
							H → L (47%)
							H → L + 1 (4%)
	2.85/434.91	0.6825					H → L (5%)
							H → L + 1 (94%)

3.4. Evaluating V_{oc} and the lifetime of the first excited state

The solar-to-electricity conversion efficiency (η) of the DSSCs is calculated from the following definition:

$$\eta = \frac{J_{sc} V_{oc} FF}{P_{in}}, \tag{4}$$

where J_{sc} is the short-circuit photocurrent density, V_{oc} is the open-circuit photovoltage, FF is the fill factor and P_{in} is the intensity of the incident light, that the J_{sc}, the V_{oc} and the FF are only obtained by experiment [13,40].

The V_{oc} for DSSCs can be expressed as:

$$V_{oc} = \frac{E_{CB}}{q} + \frac{kT}{q}\ln\left(\frac{n_c}{N_{CB}}\right) - \frac{E_{redox}}{q}, \tag{5}$$

where in this equation, q is the unit charge, E_{CB} is the conduction band edge of semiconductor, kT is the thermal energy, n_c is the electron number in the conduction band, N_{CB} is the effective density of state at the CB of TiO_2 and E_{redox} is the oxidation potential of the electrolyte. Among these parameters, kT, q, E_{redox} and N_{CB} are assumed as constants. Therefore, V_{oc} is mainly determined by the position of the conduction band edge (E_{CB}) and the n_c [11,41].

The V_{oc} corresponds to the difference between the redox potential of electrolyte and the conduction band edge of semiconductor [7]. The position of the conduction band edge of TiO_2 will be shifted by the surface adsorbed dye that is closely related to the sensitizer structure. For the same DSSCs with only different dyes, any change in the dye structure will shift the conduction band edge, and hence the V_{oc} [11,41]. The C1, C2 and S dyes adsorption effects

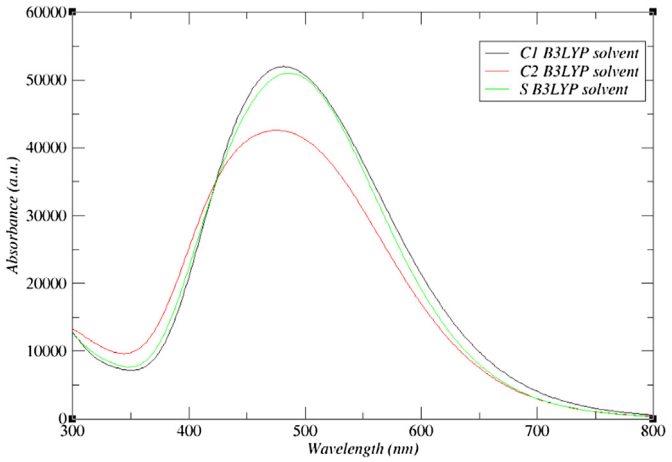

Fig. 3. Simulated absorption spectra of C1, C2 and S at the B3LYP/6-311+G(d,p) level in THF.

on conduction band shift of TiO_2 will be discussed in details in Section 3.6.

Another important parameter affecting V_{oc} is n_c, which is directly correlated with the electron injection rate (k_{inject}) [41]. The description of the electron transfer from a dye to a conduction band of the semiconductor, the rate of the charge transfer can be expressed by the Marcus electron transfer theory:

$$k_{inject} = |V_{RP}|^2 \Big/ \hbar(\pi/\lambda k_B T)^{1/2} \exp\left[-\left(\Delta G^{inject} + \lambda\right)^2 \Big/ 4\lambda k_B T \right]. \quad (6)$$

In Eq. (6), k_B is the Boltzmann thermal energy, $\hbar$ is related to Planck constant $(h/2\pi)$, λ is the reorganization energy of the system, $-\Delta G^{inject}$ is the free energy of electron injection and k_{inject} is the injection rate constant. $|V_{RP}|$ is the coupling constant between the organic dyes and the semiconductor surface. The larger $|V_{RP}|$ leads to higher rate constant which would result better dye. Hsu et al. explained that $|V_{RP}|$ can be derived from this equation:

$$|V_{RP}| = \Delta E_{RP}/2. \quad (7)$$

From Eq. (7), it is found that the higher injection driving force (ΔE_{RP}) would lead to improving the $|V_{RP}|$ which would increase the electron injection in DSSCs. The ΔE_{RP} can be evaluated by Koopmans approximation as:

$$\Delta E_{RP} = \left[E^{dye}_{LUMO} + 2E^{dye}_{HOMO}\right] - \left[E^{dye}_{LUMO} + E^{dye}_{HOMO} + E^{TiO_2}_{CB}\right]. \quad (8)$$

$E^{TiO_2}_{CB}$ is often difficult to be exactly determined because it is sensitive to the conditions, e.g. the pH of the solution. Therefore, we used the experimental value of $E^{TiO_2}_{CB}$ that is −4.0 eV corresponding to conditions where the TiO_2 is in connection with aqueous redox electrolytes of fixed pH 7.0 [41–43].

Calculated $|V_{RP}|$ (Table 5), has been observed as: S > C2 > C1. These results show that, the order of k_{inject} may approximately be expressed as: S > C2 > C1. The highest k_{inject} of the S dye compared to the other dyes, show that the S dye has the largest n_c than the other dyes and thus the highest V_{oc}. The results in Table 3 also shows that the natural charge populated in anchoring group in the S dye is more than the natural charge populated in anchoring groups in the C2 and C1 dyes. This means the more charges populated in the acceptor group of the S dye are favorable to increase the V_{oc} of the S dye. It shows that more charges populated in anchoring groups correspond to larger V_{oc} [44]. Qualitatively, all these results can show that the V_{oc} for S is higher than C2 and the V_{oc} for C2 is higher than C1 that are consistent with the experimental V_{oc} [11].

The lifetime of the first excited state was calculated using the Eq. (3) to predict the efficiency of electron injection. A dye with a longer lifetime in the excited state is estimated to be more suitable for charge transfer. To estimate the lifetime of the excited state, an assumption was made in the present investigation. Spontaneous radiation is the main competing deactivation process with electron injection and other deactivation channels such as non-radiative internal conversion, intersystem crossing from the singlet state to triplet state, electron injection, and so on can be omitted. Although this assumption is very hypothetical and it could not be expected to get exact lifetimes which are close to real values, it is possible that the comparison of the lifetimes obtained with the same assumption should give a beneficial indication of the performance of numerous similar dyes [30,31]. The calculated lifetimes of the first excited state are shown in Table 5. It can be found that the S dye with the sulfonic acid anchoring group, has the longest lifetime (8.41 ns). The lifetimes of the C1 and C2 dyes are close to each other, just C1 dye has a bit longer lifetime. The S dye with the longest lifetime is more likely a good dye for charge transfer and may have the potentially high ability in electron injection from dye to semiconductor, and thus more efficiency.

3.5. Excited state oxidation potential energy and electron injection free energy

The discussion about the electron transfer process occurring between dyes and TiO_2 surface, requires the knowledge of Rehm-Weller relationship, which was discussed in Section 2. This equation: $\Delta G^{inject} = E^{dye*}_{OX} - E^{TiO_2}_{CB}$ was used to predict the thermodynamic feasibility for electron transfer reaction [16,45]. The ground state oxidation potentials (E^{dye}_{OX}), excited state oxidation potentials (E^{dye*}_{OX}) and the electron injection free energy (ΔG^{inject}) computed at B3LYP/6-311+G(d,p) level for the C1, C2 and S dyes are shown in Table 6. The HOMO level relates to the oxidation potential of dye, and E^{dye}_{OX} can be expressed as negative E_{HOMO} [7,16].

E^{dye*}_{OX} of the dyes falls within a range 3.91–3.95, 3.81–3.86, 3.80–3.85 and 3.82–3.89 eV in vacuum, THF, dichloromethane and chloroform, respectively. E^{dye*}_{OX} of all dyes decreases from gas to solvent and its value in solvent media is in decreasing order: S > C1 > C2. It shows that the most convenient oxidizing species is C2 while S is the worst. All calculated ΔG^{inject}, is in a negative value. ΔG^{inject} in solvent media is more negative than ΔG^{inject} in the gas phase. These results indicated that the effect of dielectric surrounding to ΔG^{inject} values is huge from gas to solvent media. From the inspection of the data listed in Table 6, we can conclude that for all the dyes, there is not much difference of ΔG^{inject} in the various solvents. ΔG^{inject} in solvents with higher dielectric constant are a little more negative than ΔG^{inject} in solvents with lower dielectric constant. Dielectric constant of dichloromethane (9.1) is larger than THF (7.5) and chloroform (4.8). Thus the differences between ΔG^{inject} in the different solvents and vacuum is in decreasing order:

$$\Delta G^{inject}_{dichloromethane} - \Delta G^{inject}_{vacuum} > \Delta G^{inject}_{THF} - \Delta G^{inject}_{vacuum} > \Delta G^{inject}_{chloroform} - \Delta G^{inject}_{vacuum}.$$

As expected, the solvent stabilized electron injection driving force and oxidation potential. The negative values of ΔG^{inject} for C1, C2 and S dyes, shows that thermodynamically, the charge transfer process from the dye excited state to the conduction band of TiO_2, is spontaneous.

Table 6
Estimated ΔG^{inject}, E_{OX}^{dye*} and E_{OX}^{dye} (all in eV) for these dyes in vacuum and THF media calculated at TDDFT/B3LYP/6-311+G(d,p) level.

Dyes	E_{OX}^{dye}	Vacuum E_{OX}^{dye*}	ΔG^{inject}	E_{OX}^{dye}	THF E_{OX}^{dye*}	ΔG^{inject}	Dichloromethane ΔG^{inject}	Chloroform ΔG^{inject}
C1	6.36	3.95	−0.14	6.16	3.83	−0.27	−0.28	−0.25
C2	6.39	3.91	−0.19	6.19	3.81	−0.29	−0.30	−0.27
S	6.54	3.94	−0.16	6.25	3.86	−0.24	−0.25	−0.21

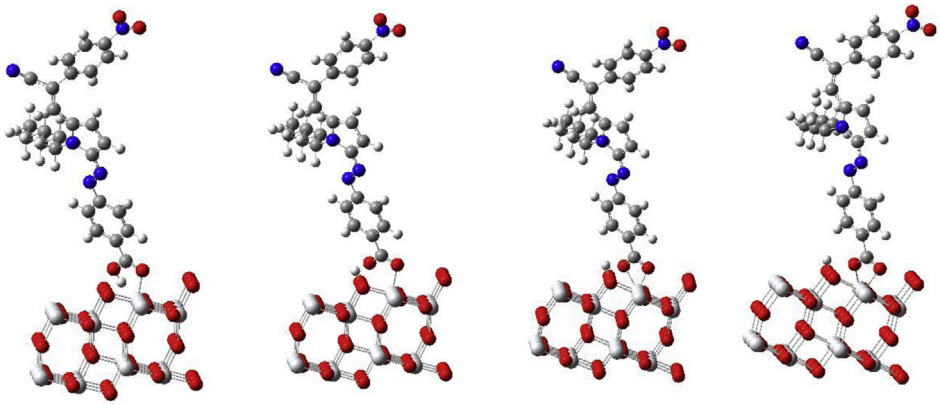

Fig. 4. Optimized geometrical structures of the C1 dye adsorbed on $(TiO_2)_{24}$.

Another factor corresponds to efficiency of DSSC is the light harvesting efficiency (LHE) of the dye. Usually, the higher LHE value, increases the photocurrent response. The LHE can be calculated from this equation:

$$LHE = 1 - 10^{-f}, \tag{9}$$

where f is the oscillator strength of the dye corresponding to λ_{max} [16,46,47]. The calculated LHE of the dyes presented in Table 5. It can be found that the LHE values are almost close to each other and the LHE of C2 is slightly higher than the other dyes. It is known that TDDFT is less efficient for the assessment of transition probabilities than for transition energies. Thus, the LHE criterion has been underweight in this study.

The exciton binding energy (EBE) is another important quantity for the efficiency of excitonic solar cells. EBE is correlated to the charge separation in solar cells and the dye with larger EBE has the lowest charge separation efficiency. EBE can be obtained as the difference between the electronic and optical band gap energies. The energy difference between the HOMO and LUMO levels is taken to be the electronic band gap, while the optical gap is approximated as first excitation energy [44,48]. The calculated EBE (in eV) of the dyes is shown in Table 5. The order of EBE is: C1 > C2 > S. It indicates that the S dye generates the smallest EBE, which is favorable for photo-to-current energy conversion. Therefore Dyes with lower EBE have higher efficiency in generating current from the absorbed light. It demonstrates an inverse relationship between the EBE and the efficiency of the dyes in DSSC devices.

3.6. Dye–TiO_2 interactions

We have also carried out theoretical calculations on the dyes adsorbed onto the TiO_2 surface. The nanocluster considered in the present work is $(TiO_2)_{24}$ with anatase (101) surface. Among the three natural forms of TiO_2: rutile, anatase and brookite, Although rutile is the thermodynamically most stable, but anatase is the preferred structure in DSSCs because of its larger band gap (3.2 vs 3.0 eV for rutile), higher conduction band energy and its easier synthesis at the nanoscale. TiO_2 nanocluster is most thermodynamically stable with the (101) surface, therefore anatase (101) has more application in DSSCs [13,49–52].

There are several possible adsorption modes of the dyes on the TiO_2 surface. The molecular monodentate structure, that the dye anchors the TiO_2 surface without deprotonation and one 5-fold coordinated Ti-atom (5c-Ti) of TiO_2 bonded to the one oxygen atom of the anchoring group of the dye. The dissociative monodentate structure that one 5c-Ti of TiO_2 linked to the one oxygen atom of the anchoring group of the dye and the acid hydrogen atom of the dye is dissociated and connected to a nearby surface 2-fold coordinated O-atom (2c-O).

Bidentate chelating (BC) which only one 5c-Ti of the TiO_2 is involved with the two O atoms of the anchoring group. Bidentate bridging (BB) that the two O atoms of the anchoring group are bound to two 5c-Ti atoms. In dissociative structures (BC and BB), the proton on anchoring group is transferred to the 2c-O atom on the surface of TiO_2 near the adsorbed site [53–56].

The optimized structures of various possible adsorption configurations are shown in Figs. 4–6. By looking at the optimized parameters that are shown in Table 7, we can find that there is an asymmetry in the O–Ti bonds in BB and BC structures that this difference in the Ti–O distances can be attributed to the presence of the proton transferred to the surface oxygen. For C1–TiO_2, in the monodentate molecular structure, the bond distances between 5c-Ti and O atom is about 1.99 Å, slightly longer than that of the dissociative monodentate structure (1.97 Å). In the bidentate structures, the two Ti–O distances are 2.01 and 2.05 Å for BB structure and 1.93 and 1.99 Å for BC configuration, which are slightly larger than that in the TiO_2 structure (1.93 Å). These Ti–O distances suggest that there is a strong chemisorption of the dye on the TiO_2 (101) surface. Very similar bond distances are obtained for the molecular monodentate, dissociative monodentate, bidentate bridging and bidentate chelating configurations of C2–TiO_2 and S–TiO_2. These results show that the average O–Ti bond length of S–TiO_2 is slightly shorter than that of C1–TiO_2 and C2–TiO_2

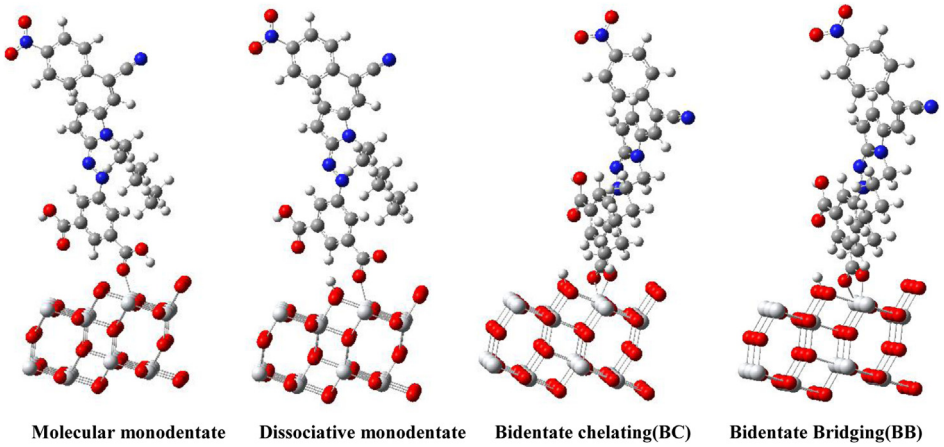

Fig. 5. Optimized geometrical structures of the C2 dye adsorbed on $(TiO_2)_{24}$.

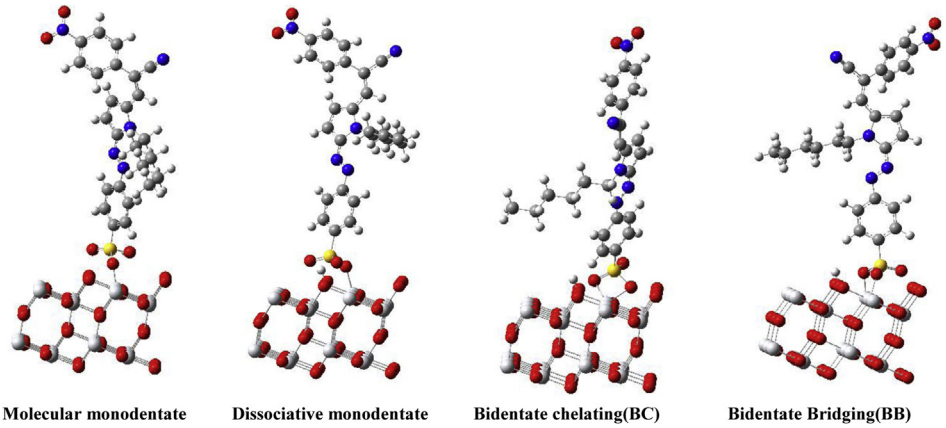

Fig. 6. Optimized geometrical structures of the S dye adsorbed on $(TiO_2)_{24}$.

structures, which indicates stronger interactions of the S dye with the TiO_2 surface and possibly stronger electronic coupling.

The calculated LUMO energy levels of the various configurations of dye–TiO_2 are shown in Table 7. After adsorption of all the dyes onto the TiO_2 surface, the LUMO level will decrease due to the interaction with TiO_2. The LUMO of the dye–TiO_2 should be located above the conduction band of TiO_2 [57–60]. The calculated LUMO energy level of TiO_2 is: −4.30 eV that is very close to the experimental conduction band of TiO_2 (−4.1 eV) [11]. From the results, it is found that in C1–TiO_2 and S–TiO_2 systems, the calculated LUMO energies of molecular monodentate, bidentate bridging and bidentate chelating are higher than the calculated conduction band of TiO_2 (−4.30 eV). In C2–TiO_2, bidentate bridging and bidentate chelating structures have the higher LUMO energy level than −4.30 eV. Therefore, we can compare the other properties in these systems between BB and BC configurations, because only BB and BC structures in each three dyes-TiO_2 have higher LUMO energy level than −4.30 eV.

The adsorption energies (E_{ads}) of dyes on the $(TiO_2)_{24}$ are calculated using the equation [53,60]:

$$E_{ads} = E_{dye} + E_{TiO_2} - E_{(dye+TiO_2),} \quad (10)$$

where E_{dye} represents the total energy of isolated dye, E_{TiO_2} is the total energy of $(TiO_2)_{24}$, and $E_{dye+TiO_2}$ is the total energy of dye–$(TiO_2)_{24}$ system. The positive value of E_{ads} shows a stable adsorption of dye on $(TiO_2)_{24}$ surface. The adsorption energies (E_{ads}) of these configurations are shown in Table 7. The values show that between bidentate bridging (BB) and bidentate chelating (BC) configurations in all these systems, BB structures have higher adsorption energy thus they are more stable than BC structures. Therefore, in these dyes the preferred adsorption mode is bidentate bridging.

The conduction band energy of the TiO_2 could be shifted by adsorbed species such as dye molecules. It is one of the essential factors affecting V_{oc}. The negative shift of the CB level of TiO_2 results in a higher V_{oc} [11,61]. On the basis of the calculated adsorption energies of different configurations of these dyes, we adopted the bidentate bridging mode. ΔE_{CB} of these dyes in BB structures are listed in Table 7. The values indicate that the order of the negative shift of the conduction band of TiO_2 as a result of the adsorption of these dyes onto the TiO_2 surface is: S > C2 > C1. i.e. ΔE_{CB} for S is higher than C2 and ΔE_{CB} for C2 is higher than C1. Thus we can conclude that the order of V_{oc} could be: S > C2 > C1 that it is according to the experimental values of V_{oc}.

4. Conclusion

In this paper, the geometries and electronic properties of the dye sensitizers C1, C2 and S both in the gas phase and in solution were studied by using DFT method with hybrid functional B3LYP and 6-311+G (d,p) basis set, and the UV–vis spectra were investigated by

Table 7
Important optimized bond lengths (Å), adsorption energies (kcal/mol), E_{LUMO} (eV) of dye–TiO_2, E_{LUMO} $(TiO_2)_{24}$, E_{LUMO} dye and CB shift ΔE_{CB} (eV) for the different adsorption configurations.

Configurations	Ti–O	Ti–O	E_{ads}	E_{LUMO}	$E_{LUMO}(TiO_2)$	E_{LUMO}(dye)	ΔE_{CB}
C1–TiO_2							
Molecular monodentate	1.99		122.51	−4.28	−4.30	−3.12	0.02
Dissociative monodentate	1.97		120.12	−4.31			
Bidentate bridging (BB)	2.01	2.05	134.86	−4.23			0.07
Bidentate chelating (BC)	1.93	1.99	25.08	−4.15			0.15
C2–TiO_2							
Molecular monodentate	1.97		143.31	−4.32	−4.30	−3.09	
Dissociative monodentate	1.94		133.04	−4.36			
Bidentate bridging (BB)	1.95	2.00	89.11	−4.21			0.09
Bidentate chelating (BC)	1.97	2.04	72.83	−3.98			0.32
S–TiO_2							
Molecular monodentate	1.94		116.27	−4.24	−4.30	−3.18	0.06
Dissociative monodentate	1.93		115.28	−4.32			
Bidentate bridging (BB)	1.94	1.99	118.01	−3.97			0.33
Bidentate chelating (BC)	2.02	2.08	5.52	−3.93			0.37

using TD-DFT methods with the hybrid functional B3LYP at the same basis set. The calculated geometries indicate that strong conjugation is formed in the dyes, which is beneficial to the intramolecular charge transfer. The NBO results suggest that there are some charges transferred from the electron donor (1-hexylpyrrole group) to the electron acceptor (substituted-phenyl-azo group) through the conjugate chemical bonds in these dyes. NBO analysis showed that the charge populated in the acceptor group of S is higher than C2 and C1 that indicates that V_{oc} for S is larger than C2 and C1. The LUMO energy levels of these dyes are higher than the conduction band edge of the TiO_2, indicating that the electron transfer from the excited dyes to the TiO_2 conduction band is possible. The ground and excited state oxidation potential energies as well as ΔG^{inject} of the dyes show that they are thermodynamically favorable in charge transfer into the conduction band of TiO_2. The HOMO energy levels of these dyes are lower than reduction potential energy of the electrolyte (I^-/I_3^-), which means when they lose electrons could be restored by getting electrons from the electrolyte. TD-DFT is a suitable method for calculating the properties of the excited state of the dyes which can be a great help in the design of new and more efficient sensitizers for future DSSCs. The electronic absorption spectra of these dyes have been studied and compared with previous experimental work. Inclusion of solvent effects increases the oscillator strength and results in red shifts of the spectra of these dyes. The blue-shift in the simulated absorption spectra with respect to the experiment may be rooted in the inherent approximations in the TD-DFT and solvent effects models. The lifetime of the first excited state of the S dye is higher than the other dyes, implying that the S dye may have more efficiency because its high ability in electron injection from dye to semiconductor. Exciton binding energy (EBE) of the S dye is smaller than the other dyes that exhibit better efficiency in DSSCs. Thus, there is an inverse relationship between the EBE and the efficiency of dyes. Theoretical calculations on dye–TiO_2 shows that the two Ti–O distances in the BB configuration of S–TiO_2 are smaller than those of in C1–TiO_2 and C2–TiO_2 that indicates a stronger interaction between the S dye and TiO_2 surface. On the basis of the LUMO energy levels and E_{ads} of these systems, BB configuration is preferred adsorption mode. The order of ΔE_{CB} is: S > C2 > C1 that indicates qualitatively the V_{oc} of the S dye is higher than that of the C2 and C1 dyes. Computational investigations on geometries, electronic structures, frontier molecular orbital energies, electronic absorption spectra of these dyes and dye–TiO_2 interactions, show that these dyes are good photosensitizers in DSSCs. The computational results confirmed the experimental results and the effective parameters in the efficiency can be qualitatively evaluated with computational methods.

Acknowledgments

We would like to thank Dr. Sabzyan for providing us with hardware and software facilities and Mr. Yavar T. Azar for helpful discussion.

References

[1] A. Modelli, P.D. Burrow, Electron attachment to dye-sensitized solar cell components: cyanoacetic acid, J. Phys. Chem. A 115 (2011) 1100–1107.
[2] B. O'Regan, M. Grätzel, A low-cost, high-efficiency solar cell based on dye-sensitized colloidal TiO_2 films, Nature 353 (1991) 737–740.
[3] J. Xu, L. Wang, G. Liang, Z. Bai, L. Wang, W. Xu, X. Shen, Conjugate spacer effect on molecular structures and absorption spectra of triphenylamine dyes for sensitized solar cells: density functional theory calculations, Spectrochim. Acta Part A 78 (2011) 287–293.
[4] M. Grätzel, Dye-sensitized solar cells, J. Photochem. Photobiol. C 4 (2003) 145–153.
[5] J. Xu, L. Zhu, L. Wang, L. Liu, Z. Bai, L. Wang, W. Xu, The effect of anchoring group number on molecular structures and absorption spectra of triphenylamine sensitizers: a computational study, J. Mol. Model. 18 (2012) 1767–1777.
[6] M. Grätzel, Conversion of sunlight to electric power by nanocrystalline dye-sensitized solar cells, J. Photochem. Photobiol. A 164 (2004) 3–14.
[7] C.-R. Zhang, L. Liu, Z.-J. Liu, Y.-L. Shen, Y.-T. Sun, Y.-Z. Wu, Y.-H. Chen, L.-H. Yuan, W. Wang, H.-S. Chen, Electronic structures and optical properties of organic dye sensitizer NKX derivatives for solar cells: a theoretical approach, J. Mol. Graph. Model. 38 (2012) 419–429.
[8] M. Pastore, S. Fantacci, F. De Angelis, Ab initio determination of ground and excited state oxidation potentials of organic chromophores for dye-sensitized solar cells, J. Phys. Chem. C 114 (2010) 22742–22750.
[9] C.-H. Yang, S.-H. Liao, Y.-K. Sun, Y.-Y. Chuang, T.-L. Wang, Y.-T. Shieh, W.-C. Lin, Optimization of multiple electron donor and acceptor in carbazole-triphenylamine-based molecules for application of dye-sensitized solar cells, J. Phys. Chem. C 114 (2010) 21786–21794.
[10] C.-R. Zhang, Z.-J. Liu, Y.-H. Chen, H.-S. Chen, Y.-Z. Wu, L.-H. Yuan, DFT and TDDFT study on organic dye sensitizers D5, DST and DSS for solar cells, J. Mol. Struct. THEOCHEM 899 (2009) 86–93.
[11] J.A. Mikroyannidis, D.V. Tsagkournos, P. Balraju, G.D. Sharma, Low band gap dyes based on 2-styryl-5-phenylazo-pyrrole: synthesis and application for efficient dye-sensitized solar cells, J. Power Sources 196 (2011) 4152–4161.
[12] O. Mostajabi Sarhangi, S.M. Hashemianzadeh, M. Moghimi Waskasi, A. Pourhassan Harzandi, A high-light-harvesting-efficiency of NKX-2593 and NKX-2883 coumarin dyes in a local electric field: can a local electric field enhance dye sensitizer solar cells efficiently? J. Photochem. Photobiol. A 225 (2011) 95–105.
[13] A. Hagfeldt, G. Boschloo, L. Sun, L. Kloo, H. Pettersson, Dye-sensitized solar cells, Chem. Rev. 110 (2010) 6595–6663.
[14] X.-H. Zhang, Y. Cui, R. Katoh, N. Koumura, K. Hara, Organic dyes containing thieno[3,2-b]indole donor for efficient dye-sensitized solar cells, J. Phys. Chem. C 114 (2010) 18283–18290.
[15] M. Moghimi Waskasi, S.M. Hashemianzadeh, O. Mostajabi Sarhangi, Significant enhancement in efficiency of NKX-2807 coumarin dye by applying external electric field in dye sensitizer solar cell: theoretical study, Comput. Theor. Chem. 978 (2011) 33–40.
[16] W. Sang-aroon, S. Saekow, V. Amornkitbamrung, Density functional theory study on the electronic structure of Monascus dyes as photosensitizer for dye-sensitized solar cells, J. Photochem. Photobiol. A 236 (2012) 35–40.
[17] J.A. Mikroyannidis, D.V. Tsagkournos, S.S. Sharma, A. Kumar, Y.K. Vijay, G.D. Sharma, Efficient bulk heterojunction solar cells based on low band gap bisazo dyes containing anthracene and/or pyrrole units, Sol. Energy Mater. Sol. Cells 94 (2010) 2318–2327.
[18] J.A. Mikroyannidis, G.D. Sharma, S.S. Sharma, Y.K. Vijay, Novel low band gap phenylenevinylene copolymer with BF2-azopyrrole complex units: synthesis

and use for efficient bulk heterojunction solar cells, J. Phys. Chem. C 114 (2010) 1520–1527.
[19] C. Jia, Z. Wan, J. Zhang, Z. Li, X. Yao, Y. Shi, Theoretical study of carbazole–-triphenylamine-based dyes for dye-sensitized solar cells, Spectrochim. Acta Part A 86 (2012) 387–391.
[20] X. Lu, C.-M.L. Wu, S. Wei, W. Guo, DFT/TD-DFT investigation of electronic structures and spectra properties of Cu-based dye sensitizers, J. Phys. Chem. A 114 (2010) 1178–1184.
[21] M.J. Frisch, G.W. Trucks, H.B. Schlegel, G.E. Scuseria, M.A. Robb, J.R. Cheeseman, J.A. Montgomery Jr., T. Vreven, K.N. Kudin, J.C. Burant, J.M. Millam, S.S. Iyengar, J. Tomasi, V. Barone, B. Mennucci, M. Cossi, G. Scalmani, N. Rega, G.A. Petersson, H. Nakatsuji, M. Hada, M. Ehara, K. Toyota, R. Fukuda, J. Hasegawa, M. Ishida, T. Nakajima, Y. Honda, O. Kitao, H. Nakai, M. Klene, X. Li, J.E. Knox, H.P. Hratchian, J.B. Cross, C. Adamo, J. Jaramillo, R. Gomperts, R.E. Stratmann, O. Yazyev, A.J. Austin, R. Cammi, C. Pomelli, J.W. Ochterski, P.Y. Ayala, K. Morokuma, G.A. Voth, P. Salvador, J.J. Dannenberg, V.G. Zakrzewski, S. Dapprich, A.D. Daniels, M.C. Strain, O. Farkas, D.K. Malick, A.D. Rabuck, K. Raghavachari, J.B. Foresman, J.V. Ortiz, Q. Cui, A.G. Baboul, S. Clifford, J. Cioslowski, B.B. Stefanov, G. Liu, A. Liashenko, P. Piskorz, I. Komaromi, R.L. Martin, D.J. Fox, T. Keith, M.A. Al-Laham, C.Y. Peng, A. Nanayakkara, M. Challacombe, P.M.W. Gill, B. Johnson, W. Chen, M.W. Wong, C. Gonzalez, J.A. Pople, Gaussian 03, Gaussian, Inc., Pittsburgh, PA, 2003.
[22] A.D. Becke, Density functional thermochemistry. III. The role of exact exchange, J. Chem. Phys. 98 (1993) 5648–5652.
[23] C. Lee, W. Yang, R.G. Parr, Development of the Colle–Salvetti correlation-energy formula into a functional of the electron density, Phys. Rev. B 37 (1988) 785–789.
[24] R. Katoh, A. Furube, T. Yoshihara, K. Hara, G. Fujihashi, S. Takano, S. Murata, H. Arakawa, M. Tachiya, Efficiencies of electron injection from excited N3 dye into nanocrystalline semiconductor(ZrO_2, TiO_2, ZnO, Nb_2O_5, SnO_2,In_2O_3) films, J. Phys. Chem. B 108 (2004) 4818–4822.
[25] C.-R. Zhang, L. Liu, J.-W. Zhe, N.-Z. Jin, L.-H. Yuan, Y.-H. Chen, Z.-Q. Wei, Y.-Z. Wu, Z.-J. Liu, H.-S. Chen, Comparative study on electronic structures and optical properties of indoline and triphenylamine dye sensitizers for solar cells, J. Mol. Model. 19 (2013) 1553–1563.
[26] H.Y. Hu, M.Z. Zhu, Z.P. Zhang, G.T. Wen, Q.X. Guo, Photoinduced electron transfer in host–guest complexes of naphthalene derivatives with p-NBCD and m-NBCD, Chin. Chem. Lett. 17 (2006) 333–336.
[27] M. Moghimi Waskasi, S.M. Hashemianzadeh, O. Mostajabi Sarhangi, A. Pourhassan Harzandi, Computational model of hydrogen production by coumarin-dye-sensitized water splitting to absorb the visible light in a local electric field, Energy Convers. Manage. 62 (2012) 154–164.
[28] C.-R. Zhang, Z.-J. Liu, Y.-T. Sun, Y.-L. Shen, Y.-H. Chen, Y.-J. Liu, W. Wang, H.-M. Zhang, Electronic structures and absorption properties of three kinds of ruthenium dye sensitizers containing bipyridine–pyrazolate for solar cells, Spectrochim. Acta Part A 79 (2011) 1843–1848.
[29] F.J. Luque, J.M. López, M. Orozco, Perspective on "Electrostatic interactions of a solute with a continuum. A direct utilization of ab initio molecular potentials for the prevision of solvent effects", Theor. Chem. Acc. 103 (2000) 343–345.
[30] L.-N. Yang, Z.-Z. Sun, S.-L. Chen, Z.-S. Li, The effects of various anchoring groups on optical and electronic properties of dyes in dye-sensitized solar cells, Dyes Pigm. 99 (2013) 29–35.
[31] S.L. Chen, L.N. Yang, Z.S. Li, How to design more efficient organic dyes for dye-sensitized solar cells? Adding more sp2-hybridized nitrogen in the triphenylamine donor, J. Power Sources 223 (2013) 86–93.
[32] R. Car, M. Parrinello, Unified approach for molecular dynamics and density-functional theory, Phys. Rev. Lett. 55 (1985) 2471–2474.
[33] A. Pasquarello, K. Laasonen, R. Car, C. Lee, D. Vanderbilt, Ab initio molecular dynamics for D-electron systems: liquid copper at 1500 K, Phys. Rev. Lett. 69 (1992) 1982–1985.
[34] P. Giannozzi, F.D. Angelis, R. Car, First-principle molecular dynamics with ultrasoft pseudopotentials: parallel implementation and application to extended bioinorganic systems, J. Chem. Phys. 120 (2004) 5903–5915.
[35] K. Sodeyama, M. Sumita, C. O'Rourke, U. Terranova, A. Islam, L. Han, D.R. Bowler, Y. Tateyama, Protonated carboxyl anchor for stable adsorption of Ru N749 dye (Black dye) on a TiO_2 anatase (101) surface, J. Phys. Chem. Lett 3 (2012) 472–477.
[36] CPMD V3.12, IBM Research Division, MPI Festkoerperforschung, Stuttgart, http://www.cpmd.org.
[37] K. Hara, T. Sato, R. Katoh, A. Furube, Y. Ohga, A. Shinpo, S. Suga, K. Sayama, H. Sugihara, H. Arakawa, Molecular design of coumarin dyes for efficient dye-sensitized solar cells, J. Phys. Chem. B 107 (2003) 597–606.
[38] P.S. Kumar, K. Vasudevan, A. Prakasam, M. Geetha, P.M. Anbarasan, Quantum chemistry calculations of 3-phenoxyphthalonitrile dye sensitizer for solar cells, Spectrochim. Acta Part A 77 (2010) 45–50.
[39] Grace-5.1.23, http://plasma-gate.weizmann.ac.il/Grace/.
[40] M. Geetha, P.S. Kumar, K. Vasudevan, A. Prakasam, G. Meenakshi, P.M. Anbarasan, Molecular modeling of 3,4-pyridinedicarbonitrile dye sensitizer for solar cells using quantum chemical calculations, J. Saudi Chem. Soc. 14 (2010) 399–407.
[41] J. Zhang, H.-B. Li, Y. Geng, S.-h. Wen, R.-L. Zhong, Y. Wu, Q. Fu, Z.-M. Su, Modification on C219 by coumarin donor toward efficient sensitizer for dye sensitized solar cells: a theoretical study, Dyes Pigm. 99 (2013) 127–135.
[42] A. Irfan, R. Jin, A.G. Al-Sehemi, A.M. Asiri, Quantum chemical study of the donor-bridge-acceptor triphenylamine based sensitizers, Spectrochim. Acta Part A 110 (2013) 60–66.
[43] A. Irfan, Quantum chemical investigations of electron injection in triphenylamine-dye sensitized TiO_2 used in dye sensitized solar cells, Mater. Chem. Phys. 142 (2013) 238–247.
[44] C.-R. Zhang, L. Liu, J.-W. Zhe, N.-Z. Jin, Y. Ma, L.-H. Yuan, M.-L. Zhang, Y.-Z. Wu, Z.-J. Liu, H.-S. Chen, The role of the conjugate bridge in electronic structures and related properties of tetrahydroquinoline for dye sensitized solar cells, Int. J. Mol. Sci. 14 (2013) 5461–5481.
[45] J. Kabatc, J. Paczkowski, The photophysical and photochemical properties of the oxacarbocyanine and thiacarbocyanine dyes, Dyes Pigm. 61 (2004) 1–16.
[46] J. Zhang, H.-B. Li, S.-L. Sun, Y. Geng, Y. Wu, Z.-M. Su, Density functional theory characterization and design of high-performance diarylamine-fluorene dyes with different π spacers for dye-sensitized solar cells, J. Mater. Chem. 22 (2012) 568–576.
[47] D. Vijay, E. Varathan, V. Subramanian, Theoretical design of core modified (oxa and thia) porphyrin based organic dyes with bridging thiophene linkers, J. Mater. Chem. A 1 (2013) 4358–4369.
[48] B.-G. Kim, C.-G. Zhen, E.J. Jeong, J. Kieffer, J. Kim, Organic dye design tools for efficient photocurrent generation in dye-sensitized solar cells: exciton binding energy and electron acceptors, Adv. Funct. Mater. 22 (2012) 1606–1612.
[49] A. Bouzoubaa, A. Markovits, M. Calatayud, C. Minot, Comparison of the reduction of metal oxide surfaces: TiO_2 – anatase, TiO_2 – rutile and SnO_2 – rutile, Surf. Sci. 583 (2005) 107–117.
[50] X.-Q. Gongi, A. Selloni, M. Batzill, U. Diebold, Steps on anatase TiO_2 (101), Nat. Mater. 5 (8) (2006) 665–670.
[51] J. Chena, F.-Q. Bai, J. Wang, L. Hao, Z.-F. Xie, Q.-J. Pan, H.-X. Zhang, Theoretical studies on spectroscopic properties of ruthenium sensitizers absorbed to TiO_2 film surface with connection mode for DSSC, Dyes Pigm. 94 (2012) 459–468.
[52] V. Blagojevic, Y.-R. Chen, M. Steigerwald, L. Brus, R.A. Friesner, Quantum chemical investigation of cluster models for TiO_2 nanoparticles with water-derived ligand passivation: studies of excess electron states and implications for charge transport in the Gratzel cell, J. Phys. Chem. C 113 (2009) 19806–19811.
[53] A. Puyad, C.R. Kumar, K. Bhanuprakash, Adsorption of croconate dyes on TiO_2 anatase (101) surface: a periodic DFT study to understand the binding of diketo groups, J. Chem. Sci. 124 (2012) 301–310.
[54] L. Ducasse, F. Castet, R. Méreau, S. Nénon, J. Idé, T. Toupance, C. Olivier, Structure and absorption properties of the C212 dye chemisorbed onto the TiO_2 (101) anatase surface, Chem. Phys. Lett. 556 (2013) 151–157.
[55] E. Mosconi, A. Selloni, F. De Angelis, Solvent effects on the adsorption geometry and electronic structure of dye-sensitized TiO_2 : a first-principles investigation, J. Phys. Chem. C 116 (2012) 5932–5940.
[56] J. Liang, C. Zhu, Z. Cao, Electronic and optical properties of the triphenylamine-based organic dye sensitized TiO_2 semiconductor: insight from first principles calculations, Phys. Chem. Chem. Phys. 15 (2013) 13844–13851.
[57] R. Sánchez-de-Armas, M.A. San Miguel, J. Oviedo, J.F. Sanz, Coumarin derivatives for dye sensitized solar cells: a TD-DFT study, Phys. Chem. Chem. Phys. 14 (2012) 225–233.
[58] W. Fan, D. Tanab, W. Deng, Theoretical investigation of triphenylamine dye/titanium dioxide interface for dye-sensitized solar cells, Phys. Chem. Chem. Phys. 13 (2011) 16159–16167.
[59] S. Agrawal, P. Dev, N.J. English, K.R. Thampi, J.M.D. MacElroy, A TD-DFT study of the effects of structural variations on the photochemistry of polyene dyes, Chem. Sci. 3 (2012) 416–424.
[60] S. Jungsuttiwong, R. Tarsang, T. Sudyoadsuk, V. Promarak, P. Khongpracha, S. Namuangruk, Theoretical study on novel double donor-based dyes used in high efficient dye-sensitized solar cells: the application of TDDFT study to the electron injection process, Org. Electron. 14 (2013) 711–722.
[61] Y. Ooyama, Y. Harima, Molecular designs and syntheses of organic dyes for dye-sensitized solar cells, Eur. J. Org. Chem. 2009 (2009) 2903–2934.